A biomimetic DNA-made channel for the ligand-controlled and selective transport of small-molecule cargo through a biological membrane

Jonathan R. Burns[1], Astrid Seifert[2], Niels Fertig[2], Stefan Howorka[1]

[1]*Department of Chemistry, Institute of Structural Molecular Biology, University College London, London, WC1H 0AJ, England, United Kingdom*

[2]*Nanion Technologies, GmbH, Munich, Germany*

Biological ion channels are molecular gatekeepers that control transport across cell membranes. Re-creating the functional principle with de-novo-designed materials is scientifically exciting and technologically relevant for sensing or drug-release[1, 2]. A key challenge in the fabrication of synthetic channels is, however, to achieve a predictable structure[2-4]. Here, we use DNA as building material[5-9] to rationally design an atomistically determined molecular valve to control when and which cargo is transported across a bilayer. The valve is able to specifically bind a ligand and in response undergo a nanomechanical change to open up the membrane-spanning channel. It also distinguishes with high selectivity the transported small-molecule cargo carrying a positive instead of a negative charge, something which has not been achieved in DNA nanotechnology before. Reflecting its functional performance, the DNA device may be used for controlled drug release, and the building of synthetic cell-like or logic ionic networks[10, 11].

The re-engineering of biological protein pore scaffolds is a successful approach[12, 13] which has led, for example, to components for label-free biosensing[14-17] and portable genome sequencing[18, 19]. Creating completely new architectures with synthetic materials can offer greater design freedom and translate into more functions and applications[20-26]. A key challenge in the de-novo design of membrane channels is, however, to achieve an atomistically defined structure of predictable nanomechanical properties[3] because the traditional building blocks of polypeptides and organic polymers are highly flexible[2, 4]. DNA, by contrast, is known to fold into pre-determined structures and is able to meet most the criteria required for creating synthetic channels[27-33]. Indeed, membrane-spanning DNA nanopores have been very

recently built to feature a central hollow barrel which is open at both ends[5-9]. The barrel is composed of six hexagonally arranged, interconnected DNA duplexes that enclose a 2 nm-wide lumen with a length ranging from 17 to 42 nm. The innovative step was the inclusion of hydrophobic anchors[5, 7, 9] to insert the negatively charged pores into the hydrophobic bilayer membrane. While of novelty and considerable interest[34, 35], the barrels do not exploit the full design flexibility offered by DNA nanotechnology and do not exhibit the higher-order functions of ion channels which can bind ligands, respond by nanomechanical opening, and select cargo for transport.

We used the simple geometric shape of an open barrel as a starting point to rationally design a nanodevice that can regulate the flux of matter across a bilayer membrane. The aim of the first design step was reduce the pore height to approximate the bilayer thickness[36] and thereby avoid structural flexibility and potential leakiness[37]. A pore height of 7 nm (Fig. 1a, NP) was achieved using a six-helix-bundle architecture with six concatenated DNA strands, each of which connects two neighboring duplexes at their termini (Fig. 1b). This connectivity is drastically simpler than classical origami[38] based on cadnano software where oligonucleotides run through multiple duplexes and cause a minimum height of approx. 15 nm[5, 38]. Our design with connections at the duplex ends also avoids traditional internal cross-overs that cause structural deviations from parallel aligned duplexes [39].

The second step was to design a molecular gate that closes one barrel entrance but re-opens the channel upon binding of a ligand. A origami plate has been previously used as a controllable lid for a DNA origami box[32]. But our molecular models supported by biophysical studies[37] suggest that the plate might be structurally too flexible and leaky

to form a tight seal. As a solution, we designed a nanodevice that features in its closed state, NP-C (Fig. 1c), a simple "lock" strand which is bound closely to the entrance by hybridization to two docking sites. The sites are formed by the extension of two duplex staves. Importantly, a "key" can hybridize to the lock and physically remove it to render the device in the open state, NP-O (Fig. 1c). Based on the dimension of a 2 nm channel we expected the device to regulate the flow of small organic molecules which includes many medically important drug compounds. As a final design step, we equipped the nanodevices with hydrophobic cholesterol groups (Fig. 1d) to anchor the hydrophilic nanostructures into the lipid bilayer (Fig. 1c).

We implemented our design by first constructing NP (Fig. 1a) to test if two crossovers per stave are sufficient to form a stable channel. As an additional motivation, the pore was built to serve as a reference standard for the structural derivatives NP-C and NP-O. Pore NP was assembled by annealing within 15 min six oligonucleotides of 50 nt length (Supplementary Tables S1 and S2, Figs. S1-S3). The assembly was complete as demonstrated by a single band in gel electrophoresis for pores with and without lipid anchors (Fig. 2a, lane 1 and 2, respectively). SDS was added to the electrophoresis buffer to avoid band smearing[6] caused by the hydrophobic lipid anchors (Fig. S3)[9]. The successful formation of the barrel was also supported by faster migrating control samples with incomplete sets of DNA strands (Fig. 2a, lanes 4 to 7). Atomic force microscopy of NP (Fig. 2b) yielded a length and width of 9.0 ± 1.5 nm and 5.1 ± 1.1 nm (full width at half maximum, n = 15), respectively, in agreement with the dimensions of the pore after correcting for tip broadening[40]. To support the determination of the pore width, we examined variant $NP_{short\ loop}$ with shortened loops between the duplexes. The blunt-ended pore termini enabled base π-stacking between

head-to-tail assembled pores as seen in AFM analysis (Fig. 2b, Fig. S4). The resulting 50 nm-long features had a width of 6.8 ± 1.3 nm (n = 16), but only exist at the solid interfaces but not in solution. To test whether regular NP pores with lipid anchors insert into bilayers, we determined the melting temperature of the DNA barrel. Consistent with membrane interaction, the melting temperature, T_m, increased by approx. 5 °C (Fig. 2c) while pores without anchors were unaffected (Fig. S5).

Single-channel current recordings were used to examine whether NP is membrane-spanning and structurally stable in the bilayer. A positive outcome would validate our non-traditional DNA architecture. NP formed a stable channel across the membrane as shown by a steady current in a representative current trace at +40 mV (Fig. 2d) and a narrow distribution of conductances (Fig. 2e; mean of 1.62 ± 0.09 nS, n = 100). The pore is also of ohmic behavior (Fig. S6) reflecting its vertical symmetry. Additional recordings in the presence of poly(ethylene glycol) (PEG) of known hydrodynamic diameter were used to confirm the expected channel width of the NP lumen. The basis of the approach is that polymers smaller than the channel width partition into pore to reduce its conductance while larger PEG probes unable to migrate into the lumen do not block conductance. Indeed, smaller PEGs such as those with a molecular mass of 200 lowered the current compared to large polymers (Fig. 2f, Fig. S7) as summarized in a plot of the relative current change versus the hydrodynamic diameter of PEG (Fig. 2g). The upper transition point of 1.8 nm is the PEG size that is just too big to enter the pore and closely matches the expected channel width of 2.0 nm.[8] The hour-long recordings -comprising repeated addition of PEG solutions followed by washing out- also confirmed that the pore can stay open under testing conditions without collapsing (Fig. S7). At potentials higher than 60 mV, NP adopted a lower

conductance state (Fig. S6) which does not affect functionality as the NP-derived nanodevice is operated via a ligand at zero potential.

After confirming the design principle, we tested the fabrication of ligand-triggered nanopore NP-C. The device features a lock at the channel entrance (Fig. 1c) and was built by annealing the component DNA strands including the six DNA barrel strands and the lock oligonucleotide (Tables S1, S2; Figs. S1, S2). Self-assembly of NP-C was complete as shown by a single band in gel electrophoresis (Fig. 3a). Similarly, open-state NP-O was formed by annealing the six barrel strands (Tables S1, S2; Figs. S1, S2) yielding a single band (Fig. 3a) which migrated at a different height to NP-C. Accompanying FRET analysis demonstrated that NP-C was converted into NP-O by adding the key oligonucleotide to trigger the nanomechanical removal of lock DNA (Fig. 3b, Fig. S8). The signal of the acceptor positioned at the lock increased (Fig. 3b, red) while the signal for the donor at the docking site increased (Fig. 3b, blue). The key-and-lock interaction was specific because a key with non-matching sequence (Table S1) did not lead to a change (data not shown). The key-induced transition from NP-C to NP-O was also confirmed with gel electrophoresis (Fig. S8).

To prove that the lock is obstructing the channel entrance, we conducted nanopore recordings of NP-C as well as NP-O for comparison. Indeed, blocked NP-C had a lower conductance of 0.66 ± 0.06 nS (n = 27, Figs. 3c-1 and 3c-2) than open NP-O with 1.34 ± 0.08 (n = 29, Figs. 3d-1 and 3d-2). The lock in NP-C did not completely abolish the pore current due to small 0.2-nm sized gaps between the pore wall and the lock (Fig. S2) as well as the ion permeability of the DNA channel wall[37]. The molecular difference at the channel entrance was also apparent in the electronic

signature of current traces recorded at a steady voltage (Fig. 3c-1 and Fig. 3d-1) and for a voltage ramp from -100 to +100 mV (Fig. 3c-3 and Fig. 3d-3). While NP-C was electrically quiet (Fig. 3c-1 and 3c-3), NP-O was noisier (Fig. 3d-1) and featured very frequent and short downward spikes at a positive potential (Fig. 3d-3). The spikes are probably caused by the electrophoretically induced flapping of negatively charged docking sites towards the positive potential at the *trans* pore side (Fig. 3d-3, Figs. S9 and S10), something which cannot occur when the docking sites are held static by the lock in NP-C (Fig. 3c-3, Fig. S11). These recordings are striking because they offer a unique view of the molecular and dynamic properties of the rationally designed nanopores at the single-molecule level. Under the conditions used for current recordings the pores inserted in two different orientations into membranes (Figs. S9-11). Directional insertion was not the focus of this study but can be achieved by placing hydrophobic anchors at one pore terminus[7, 9].

With the molecular characterization of NP-C and NP-O in place, the next step was to investigate the use of NP-C for controlling the release of small-molecule cargo from lipid vesicles. We first used open-channel NP-O to establish whether and which molecules can pass the pore. Fluorophores were chosen as cargo due to their simple detection and their ability to mimic the release of small molecules such as drugs. In the transport assay, the fluorophores are self-quenched at high-concentrations inside the vesicles but increase in emission and absorbance upon nanopore-mediated release into the solvent (Fig. 4a; Fig. S12, S13). NP-O displayed a remarkable ability to detect charge in the cargo. For example, fluorophore sulfo-rhodamine B (SRB) with one positive and two negative charges (Fig. 4a, green; maximum size of 0.7 nm) transported successfully (Figs. 4b and 4c, green). By contrast, replacement of the

positive with a negative charge such as in 6-carboxyfluorescein (CF) of the same parent structure (Fig. 4a, red) reduced the transport, as determined from the net increase of fluorescence between the begin and end of the release curves (Figs. 4b and 4c, red; Fig. S13). The electrostatic selection of the DNA nanopore is due to its negatively charged wall because the protein pore α-hemolysin (α-HL) with an almost charge-neutral lumen of diameter ranging from 1.3 to 2.9 nm[41] did not distinguish the two fluorophores (Fig. 4c). The very low transport of CF through NP-O furthermore strongly indicates that pore insertion into vesicles did not cause major vesicle rupturing or fluorophore leakage, even though a minor effect cannot be ruled out.

Having established the cargo-selecting properties with NP-O, the successful lock-and-key mechanism was investigated with NP-C. Using SRB as a probe molecule, we examined whether the nanodevice can control transmembrane transport in response to the DNA key (Fig. 4a). Vesicles carrying closed-state NP-C that were exposed to a mismatched key only showed a very small flux (Fig. 4d) in line with expectations that the lock would block the passage (Fig. 1c). Adding matching key to convert NP-C to open state NP-O, however, led to a 140-fold increase in flux, consistent with the sequence-specific removal of the lock from the nanodevice. The analysis of flux also confirmed that NP-O has a 130-fold higher selectivity (Fig. 4d) for probe SRB over CF which differed solely by the replacement of a positive with a negative charge.

We have successfully developed a bio-inspired nanomechanical device to achieve the sequence-specific and controlled release of small-molecule cargo from vesicle containers. The next-generation nanopore advances the field of artificial DNA channels as it combines ligand-triggered channel opening and high selectivity for

small-molecule cargo[5-10]. The functional performance – as judged by the high difference in flux between closed and open channel, and for transported molecules differing by the presence of a positive or negative charge- matches or exceeds natural templates. Key to the successful fabrication of the channel were the favorable properties of DNA as a predictable and simple-to-handle building material for de-novo design. In addition, the smallest DNA channel to date[5-9] translates into high yields and low material costs to facilitate in future easy adoption of the technology by other scientists. The artificial ligand channel extends the range of biomimetic DNA materials which include molecular motors,[33, 42] antibodies[43] and multi-enzyme complexes[29, 44]. The principle of triggered opening may be used to facilitate transport of larger molecules, after adapting pore geometry. Similarly, the present ion selectivity imposed by the negatively charged DNA pore walls could be altered using nucleic acid analogues with a neutral backbone or positively charged bases. In conclusion, our report establishes the benefits of using DNA for the construction of advanced functional synthetic bilayer nanochannels. It thereby synergistically combines three exciting research areas of DNA nanotechnology, nanopores, and single-molecule research, and addresses the demand for functional DNA nanostructures.

Acknowledgements: Funded by the Leverhulme Trust (RPG-170), UCL Chemistry, and the BBSRC (grant ref. BB/M012700/1). We thank Alice Pyne and Bart Hoogenboom from the London Centre for Nanotechnology for assistance in the AFM analysis of DNA nanopores.

Author contributions: J.B. carried out all experiments except nanopore recordings which were conducted by A.S. N.F. co-supervised A.S. S.H. conceived the project, supervised J.B. and A.S., and wrote the manuscript with data input from J.B. and A.S.

Competing financial interests: There are no competing finanical interests.

References:

1. Litvinchuk, S. et al. Synthetic pores with reactive signal amplifiers as artificial tongues. *Nat. Mater.* **6**, 576-580 (2007).
2. Mayer, M. & Yang, J. Engineered ion channels as emerging tools for chemical biology. *Acc. Chem. Res.* **46**, 2998-3008 (2013).
3. Thomson, A.R. et al. Computational design of water-soluble alpha-helical barrels. *Science* **346**, 485-488 (2014).
4. Sakai, N. & Matile, S. Synthetic ion channels. *Langmuir* **29**, 9031-9040 (2013).
5. Burns, J., Stulz, E. & Howorka, S. Self-assembled DNA nanopores that span lipid bilayers. *Nano Lett.* **13**, 2351-2356 (2013).
6. Burns, J.R., Al-Juffali, N., Janes, S.M. & Howorka, S. Membrane-spanning DNA nanopores with cytotoxic effect. *Angew. Chem. Int. Ed.* **53**, 12466-12470 (2014).
7. Burns, J.R. et al. Lipid bilayer-spanning DNA nanopores with a bifunctional porphyrin anchor. *Angew. Chem. Int. Ed.* **52**, 12069–12072 (2013).

8. Seifert, A. et al. Bilayer-spanning DNA nanopores with voltage-switching between open and closed state. *ACS Nano* **9**, 1117-1126 (2015).

9. Langecker, M. et al. Synthetic lipid membrane channels formed by designed DNA nanostructures. *Science* **338**, 932-936 (2012).

10. Maglia, G. et al. Droplet networks with incorporated protein diodes show collective properties. *Nat. Nanotechnol.* **4**, 437-440 (2009).

11. Villar, G., Graham, A.D. & Bayley, H. A tissue-like printed material. *Science* **340**, 48-52 (2013).

12. Chowdhury, S., Jarecki, B.W. & Chanda, B. A molecular framework for temperature-dependent gating of ion channels. *Cell* **158**, 1148-1158 (2014).

13. Kocer, A., Walko, M., Meijberg, W. & Feringa, B.L. A light-actuated nanovalve derived from a channel protein. *Science* **309**, 755-758 (2005).

14. Howorka, S. & Siwy, Z. Nanopore analytics: Sensing of single molecules. *Chem. Soc. Rev.* **38**, 2360-2384 (2009).

15. Bayley, H. & Cremer, P.S. Stochastic sensors inspired by biology. *Nature* **413**, 226-230 (2001).

16. Wang, Y., Zheng, D., Tan, Q., Wang, M.X. & Gu, L.Q. Nanopore-based detection of circulating microRNAs in lung cancer patients. *Nat. Nanotechnol.* **6**, 668-674 (2011).

17. Wei, R.S., Gatterdam, V., Wieneke, R., Tampe, R. & Rant, U. Stochastic sensing of proteins with receptor-modified solid-state nanopores. *Nat. Nanotechnol.* **7**, 257-263 (2012).

18. Cherf, G.M. et al. Automated forward and reverse ratcheting of DNA in a nanopore at 5-angstrom precision. *Nat. Biotechnol.* **30**, 344-348 (2012).

19. Manrao, E.A. et al. Reading DNA at single-nucleotide resolution with a mutant MspA nanopore and phi29 DNA polymerase. *Nat. Biotechnol.* **30**, 349-353 (2012).

20. Traversi, F. et al. Detecting the translocation of DNA through a nanopore using graphene nanoribbons. *Nat. Nanotechnol.* **8**, 939-945 (2013).

21. Geng, J. et al. Stochastic transport through carbon nanotubes in lipid bilayers and live cell membranes. *Nature* **514**, 612-615 (2014).

22. Wanunu, M. et al. Rapid electronic detection of probe-specific microRNAs using thin nanopore sensors. *Nat. Nanotechnol.* **5**, 807-814 (2010).

23. Powell, M.R., Cleary, L., Davenport, M., Shea, K.J. & Siwy, Z.S. Electric-field-induced wetting and dewetting in single hydrophobic nanopores. *Nat. Nanotechnol.* **6**, 798-802 (2011).

24. Yusko, E.C. et al. Controlling protein translocation through nanopores with bio-inspired fluid walls. *Nat. Nanotechnol.* **6**, 253-260 (2011).

25. Di Fiori, N. et al. Optoelectronic control of surface charge and translocation dynamics in solid-state nanopores. *Nat. Nanotechnol.* **8**, 946-951 (2013).

26. Schneider, G.F. et al. Tailoring the hydrophobicity of graphene for its use as nanopores for DNA translocation. *Nat. Commun.* **4**, 2619 (2013).

27. Zheng, J. et al. From molecular to macroscopic via the rational design of a self-assembled 3D DNA crystal. *Nature* **461**, 74-77 (2009).

28. Rothemund, P.W. Folding DNA to create nanoscale shapes and patterns. *Nature* **440**, 297-302 (2006).

29. Fu, J. et al. Multi-enzyme complexes on DNA scaffolds capable of substrate channelling with an artificial swinging arm. *Nat. Nanotechnol.* **9**, 531-536 (2014).

30. Wollman, A.J., Sanchez-Cano, C., Carstairs, H.M., Cross, R.A. & Turberfield, A.J. Transport and self-organization across different length scales powered by motor proteins and programmed by DNA. *Nat. Nanotechnol.* **9**, 44-47 (2014).

31. Sacca, B. & Niemeyer, C.M. Functionalization of DNA nanostructures with proteins. *Chem. Soc. Rev.* **40**, 5910-5921 (2011).

32. Andersen, E.S. et al. Self-assembly of a nanoscale DNA box with a controllable lid. *Nature* **459**, 73-76 (2009).

33. Omabegho, T., Sha, R. & Seeman, N.C. A bipedal DNA Brownian motor with coordinated legs. *Science* **324**, 67-71 (2009).

34. Krishnan, S. & Simmel, F.C. Nanotechnology: deadly DNA. *Nat. Chem.* **7**, 17-18 (2014).

35. Eisenstein, M. Molecular engineering: Changing the channel. *Nat. Methods* **10**, 10-11 (2013).

36. Tristram-Nagle, S. et al. Structure and water permeability of fully hydrated diphytanoylPC. *Chem. Phys. Lipids* **163**, 630-637 (2010).

37. Yoo, J. & Aksimentiev, A. In situ structure and dynamics of DNA origami determined through molecular dynamics simulations. *Proc. Natl. Acad. Sci. U S A* **110**, 20099-20104 (2013).

38. Douglas, S.M. et al. Rapid prototyping of 3D DNA-origami shapes with caDNAno. *Nucleic Acids Res.* **37**, 5001-5006 (2009).

39. Bai, X.C., Martin, T.G., Scheres, S.H. & Dietz, H. Cryo-EM structure of a 3D DNA-origami object. *Proc. Natl. Acad. Sci. U S A* **109**, 20012-20017 (2012).

40. Leitner, M. et al. Single-molecule AFM characterization of individual chemically tagged DNA tetrahedra. *ACS Nano* **5**, 7048-7054 (2011).

41. Song, L. et al. Structure of staphylococcal alpha-hemolysin, a heptameric transmembrane pore. *Science* **274**, 1859-1866 (1996).

42. Wickham, S.F. et al. A DNA-based molecular motor that can navigate a network of tracks. *Nat. Nanotechnol.* **7**, 169-173 (2012).

43. Rinker, S., Ke, Y.G., Liu, Y., Chhabra, R. & Yan, H. Self-assembled DNA nanostructures for distance-dependent multivalent ligand-protein binding. *Nat. Nanotechnol.* **3**, 418-422 (2008).

44. Wilner, O.I. et al. Enzyme cascades activated on topologically programmed DNA scaffolds. *Nat. Nanotechnol.* **4**, 249-254 (2009).

Figure legends

Figure 1. A rationally designed DNA nanopore features a nanomechanical and sequence-specific gate to regulate transmembrane flux. (a) Structural model of pore NP composed of six DNA strands alternatively in dark and pale blue. The pore carries on its outside cholesterol-based membrane anchors (orange). (b) 2D map illustrating the connectivity of the six DNA strands of pore NP. (c) The "lock" DNA (red) of the closed nanopore NP-C is hybridizing to "key" DNA (green) to release open channel NP-O. (d) Chemical structure of the cholesterol membrane anchor.

Figure 2. Nanopore NP is of the expected dimensions and spans a lipid bilayer, thereby confirming the validity of the novel pore design. (a) SDS PAGE analysis of NP with (lane 1) and without cholesterol anchors (lane 2), and 1.2 % native agarose gel electrophoresis of cholesterol-free NP (lane 3) and assemblies with five to two components strands (lanes 4 to 7). (b) Atomic force micrograph of NP (left) and $NP_{short\ loop}$ (right) with a height of 1.6 ± 0.3 nm (n = 15) and 1.3 ± 0.8 nm (n = 16), respectively, caused by tip compression[40]. Scale bar = 25 nm. (c) Melting profile of cholesterol-bearing NP in the absence (blue; Tm = 50.3 ± 0.7 °C, n = 3) and presence of lipid vesicles (red; Tm = 55.2 ± 0.9 °C, n = 3). (d) Representative ionic current trace of a single NP pore in 1 M KCl, 10 mM HEPES pH 8.0 and at +40 mV relative to the *cis* side of the membrane which is defined in Fig. 1c. (e) Histogram of channel conductances obtained from 100 independent single-channel recordings at +20 mV. (f) Current traces of individual pores in the absence and presence of PEG molecules of noted mean molecular mass recorded at +20 mV. (g) The pore blockade depends on the hydrodynamic diameter of PEG. The data were derived from seven

independent measurements for PEG 62, four for PEG 200 to 400, and three for PEG 600 to 3350.

Figure 3. **A DNA key leads to the triggered opening of NP-C to yield NP-O and both pores have distinct and expected molecular properties.** (a) SDS PAGE analysis of NP-C and NP-O. (b) The addition of a five-molar excess of oligo key changes the FRET signal of NP-C. In line with a removal of key, the signal of the donor (blue) at the pore increases while the signal of the acceptor (red) positioned at the lock decreases. (c, d) Analysis via current recording of nanopores NP-C (c) and NP-O (d) with representative single-channel current traces at +40 mV for NP-C (c-1) and -40 mV for NP-O (d-1), conductance histogram analysis (c-2, d-2), and current traces for voltage ramps from -100 mV to +100 mV (c-3, d-3). Data in panel c-2 and d-2 were from 27 and 29 pores, respectively. The insets in c-3 and d-3 show the IV curves of each 10 pores. The lower conductance of NP-O compared to bare NP (1.61 ± 0.09 nS) is explained by the free docking sites which can reduce access of electrolyte ions to the channel entrance.

Figure 4. NP-C can control the DNA-triggered and charge-selective release of small-molecule cargo from a reservoir. (a) Scheme illustrating the assay to determine gating and selectivity in pore transport. Fluorophore carboxy-fluorescein (CF; red) and sulfo-rhodamine B (SRB; green) are self-quenched at high concentration inside lipid vesicles but increase their emission upon release and dilution. (b) Traces plotting fluorescence emission of CF and SRB for vesicles with inserted NP-O. (c) Histogram summarizing the release of fluorophores from NP-O and the neutral protein pore α-hemolysin (α-HL). The percentage release is

fluorescence at the end point of the kinetic curve, subtracted by the initial fluorescence at time zero and normalized to the maximum signal obtained from the detergent-lysed vesicles (Fig. S13). (d) Histogram for the flux of CF and SRB through NP-C exposed to a mismatching key, and NP-C after addition of matching key to yield NP-O. The flux is defined as the percentage release per min, as obtained from the linear fits to the initial slope of kinetic release traces. The data in c and d represent the averages and standard deviations from three independent experiments.

Figure 1

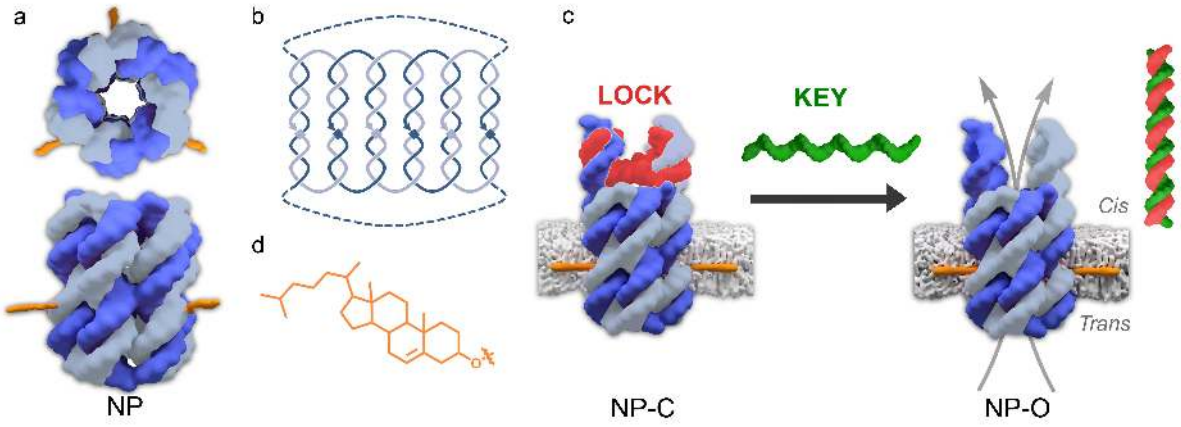

Figure 2

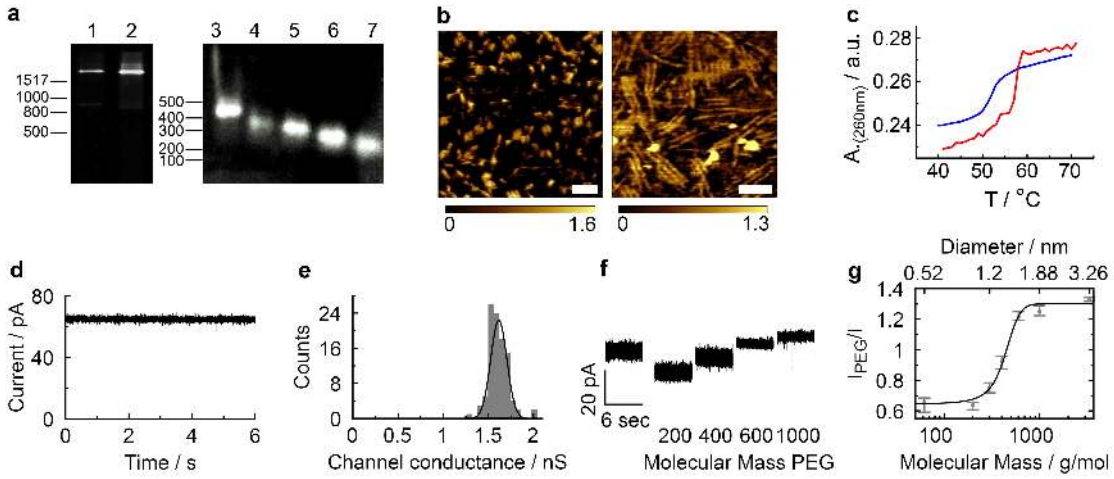

Figure 3

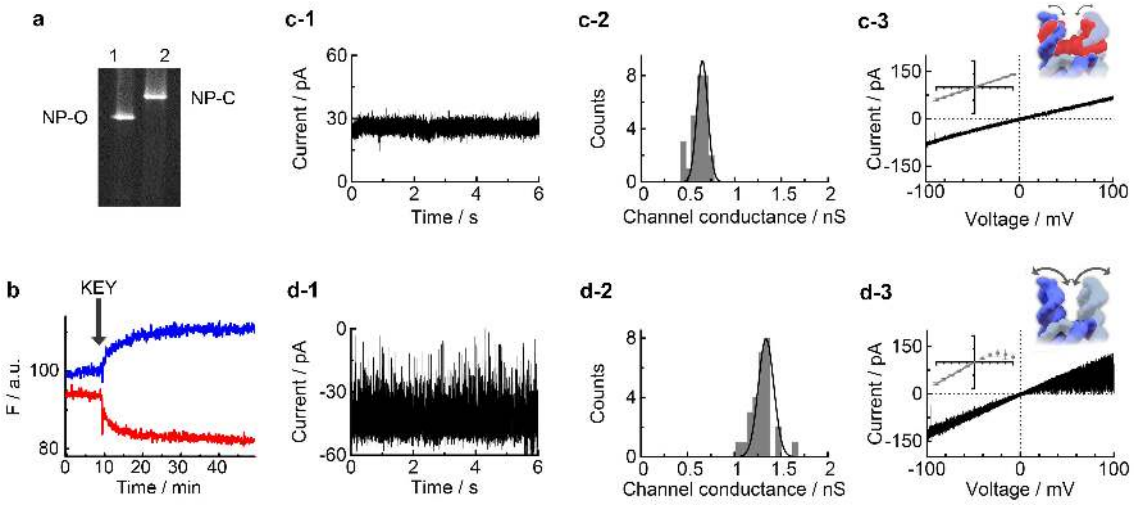

Figure 4